A Hierarchical System Design for detection of Glaucoma from Color Fundus Images

Thesis submitted in partial fulfillment
of the requirements for the degree of

MS by Research
in
Electronics & Communication

by

Madhulika Jain
200831007
madhulika.jainug08@students.iiit.ac.in

International Institute of Information Technology
Hyderabad - 500 032, INDIA
July 2015

International Institute of Information Technology
Hyderabad, India

CERTIFICATE

It is certified that the work contained in this thesis, titled "A Hierarchical System Design for detection of Glaucoma from Color Fundus Images" by Madhulika Jain, has been carried out under my supervision and is not submitted elsewhere for a degree.

_____ _____

Date Adviser: Prof. Jayanthi Sivaswamy

To My Parents, My Brother and My Guide

Acknowledgments

This thesis would not have been possible without the support of many people. Many thanks to my guide and mentor, Dr. Jayanthi Sivaswamy who read my numerous revisions and helped make some sense of every confusion whenever required. She constantly inspired me to be better at my work. Also thanks to my lab mates, Ujjwal, Arunava, Akhil, Harshit who offered guidance and help through discussions about work in particular and life in general. This acknowledgement would not be complete without thanking my parents and brother who have constantly supported me through tough times in my research and shown understanding at all times given the variable duration of dual degree in the institute. I would also like to thank my numerous friends, Nishant, Abhishek, Govind, Shandi, Roopak, Choyal, Deepshikha, Anura, Charvi, Tyagi, Bahl, Sagar, Apoorv, Shanks, Jaspal, Dhingra, who supported me in this long process and always offered help in whichever way they could.

Abstract

Glaucoma is an eye disorder which is prevalent in the aging population and causes irreversible loss of vision. Hence, computer aided solutions are of interest for screening purposes. Glaucoma is indicated by structural changes in the optic disc (OD), loss of nerve fibres and atrophy of the peripapillary region of the OD in retina. In retinal images, most of these appear in the form of subtle variation in appearance. Hence, automated assessment of glaucoma from colour fundus images is a challenging problem. Prevalent approaches aim at detecting the primary indicator, namely, the optic cup deformation relative to the disc and use the ratio of the two diameters in the vertical direction, to classify images as normal or glaucomatous.

We explore the use of global motion pattern-based features to detect glaucoma from images and propose an image representation that serves to accentuate subtle indicators of the disease. These global image features are then used to identify normal cases effectively. The proposed method is demonstrated on a large image dataset consisting of 1845 images annotated by 3 medical experts. The global approach is extended to detect atrophy and two hierarchical system designs are proposed. In the first design, only global analysis is used, while in the second both global and local analysis are employed.

In the first design, the first stage is based on features capturing information mainly of primary indicators while the second stage is based on features extracted for detecting atrophy (secondary visual indicator).

The second design attempts to combine the strengths of global and local analysis of the OD region. Global features are used to remove as many normal cases as possible in the first stage and local features are used to perform a finer classification in the second stage. This system has been tested on 1040 images with ground truth collected from 3 glaucoma experts. The results show the hybrid approach offers a good solution for glaucoma screening from retinal images

Contents

List of Figures

List of Tables

Chapter 1

Introduction

Glaucoma, a retinal disease, is one of the leading causes of blindness worldwide. It is a degenerative optic neuropathy which leads to gradual loss of retinal nerve fibre which can not be revitalized. Thus, untreated glaucoma has a potential to cause irreparable damage to retina. This irreversible and asymptomatic nature of the disease emphasizes the need for its timely detection as detecting it in early phases helps in curbing its progression through proper medication.

The proliferation of glaucoma cases in recent years adds to the growing concern towards the treatment of the disease. It prevails mainly in aging population of urban regions. It is estimated to affect 79 million people in the world by the year 2020 [5] [16] showing a 33% increase in the numbers within a decade [31]. Thus, screening for glaucoma is crucial, owing to the nature, for the early detection and enabling effective treatment in early stages to prevent permanent blindness.

The screening scenarios are practically very different from regular clinical diagnosis where glaucoma experts directly examine neuroretinal rim using an ophthalmoscope [20] or give decision based on digital retinal images obtained by HRT (Heidelberg Retina Tomograph) [21]. Unlike clinical diagnosis, the screening process is expected to face some serious challenges as it involves checkup of every individual of a community including health assessment of people in good health also, a group which is generally large. The challenges are more in India given the prevalence of the disease in population accomodating 20% glaucoma affected population of the world [31].

According to Glaucoma society of India, glaucoma is the second leading cause of blindness in India. (see Fig.1.1). The major challenge posed by Indian population is the number. At present, 12 million people in India are affected by glaucoma which is expected to increase to 16 million by 2020 [31]. The number of patients per ophthalmologist is around 2 to 3 lakhs in India. Thus apart from cost, lack of manpower in terms of skilled technicians poses major challenge in such scenarios.

Cost effective computer based diagnostic systems can reduce this requirement to a great extent and assist medical experts in diagnosis. Automated screening systems based on retinal(fundus) image analysis can aid in reducing time and effort wasted on analysis of healthy people. Such systems can classify a given case as normal (free of glaucoma related symptoms) or glaucomatous. Consequently, only those patients deemed suspect by the system need to be referred to an ophthalmologist. Thus, the classifica-

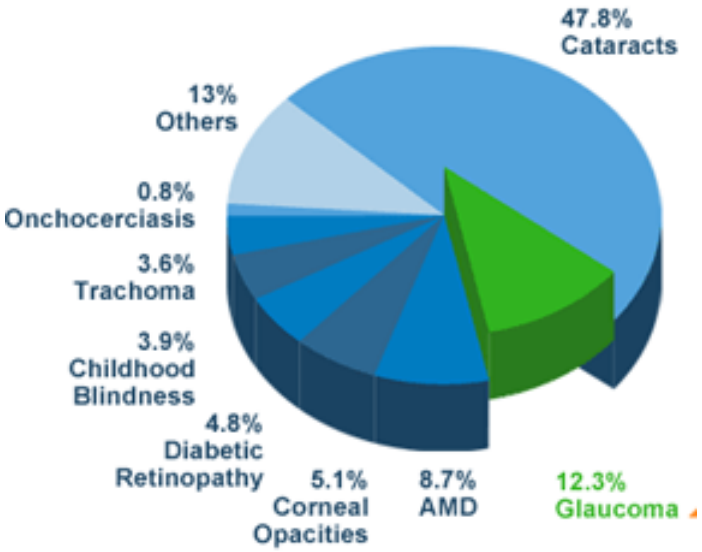

Figure 1.1 The chart shows prevalence of vision impairment in India (*image from Glaucoma Society of India*)

tion of retinal images as normal and glaucomatous is a problem of clinical significance in population screening.

1.1 Screening of Glaucoma

Manual screening of disease is performed as a public health initiative for the management of disease in a community. It refers to a proactive strategy to deal with the disease, the symptoms of which are not yet surfaced or recognized. Glaucoma screening systems is prevalent in many countries [13] [12]. Clinically, a patient is classified to be a glaucoma suspect based on various measures such as optic disc topography, visual fields, intraocular pressure, family history etc. In screening process, color retinal imaging are the *de facto* standard for screening the presence of different types of retinopathy due to its low cost, non-invasiveness and ease of use [30]. It has resulted in higher penetrability to every section of society and thereby reducing the cases of loss of vision.

Color retinal images provide two dimensional projection of retina yielding structural information of optic disc(OD) along with other retinal structures such as cup,rim and blood vessels (shown in Fig.1.2).

Since loss of nerve fibres primarily leads to glaucoma, the region of interest is the Optic disc and its periphery (Figure.1.2). An optic disc region consists of two structures: the disc identified by the outer boundary of disc (marked in white) and the cup which is within the inner boundary of optic disc. Glaucoma primarily leads to structural changes in the OD resulting in deformation of the cup and disc morphology. A common deformation is the enlargement of cup with respect to the disc and is referred

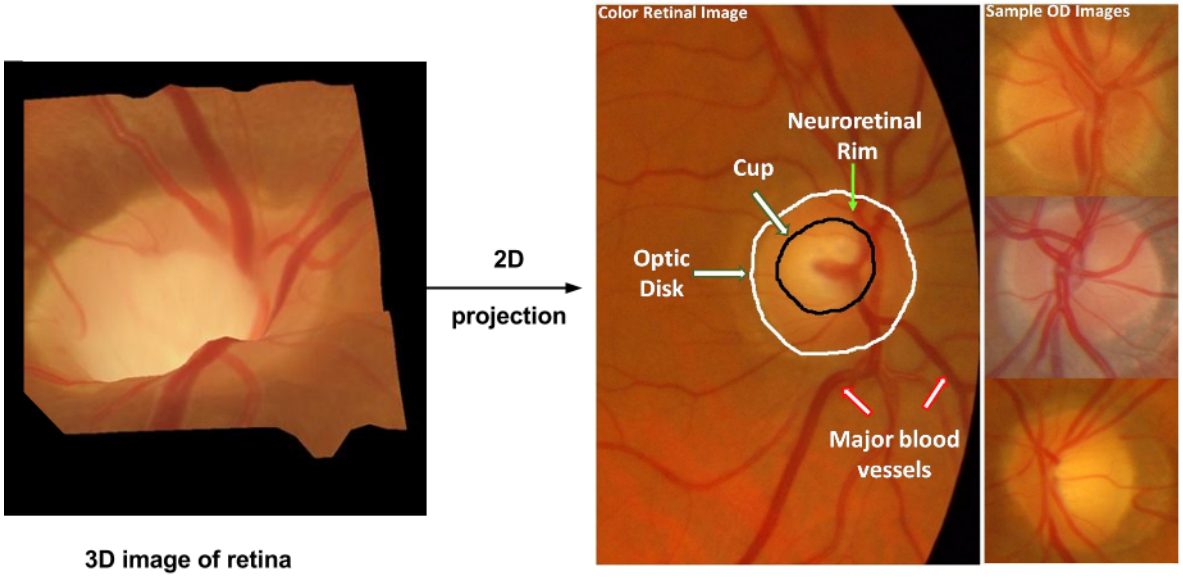

Figure 1.2 Sample 3D color image of retina (left),Sample color retinal image with optic nerve head and other retinal structures (middle), Sample region of interest with varying color, texture, disc boundary shape and surrounding deformations (right).

to as cupping (Fig.1.3). Secondary visual indicators (Fig.1.3 and 1.5) for the disease are appearance of bright blob-like lesions adjoining the OD (Peri-papillary Atrophy) and subtle darkening in a wedge-shaped region (retinal nerve fibre loss) in superior and inferior directions around the optic disc.

1.1.1 Neuroretinal Rim Thinning

In a retinal image, neuroretinal rim thinning is a definite indicator of glaucoma. The rim begins to thin with the onset of disease as the cup boundary starts approaching the disc. As a result the cup-to-disc diameter ratio increases. Thinning can be a global or local phenomenon around the cup boundary. Fig.1.3 shows an example of global rim thinning in the second row. It can be noted that nearly the entire boundary along the cup is extended to the disc in this case. Fig.1.4 shows an example where only a small local region in the rim has undergone thinning. Here, thinning is a subtle variation in the ill-defined cup boundary. While easily visible to a trained human eye, automatic detection of such minor variations across retinal images, already inflicted with other non-disease variations is a significant challenge.

1.1.2 Peripapillary Atrophy (PPA)

PPA is another indicator for glaucoma (see Fig1.4(in yellow)). While the cup boundary is not affected due to this, a change in intensity adjoining the disc boundary can be observed clearly. PPA occurs due to atrophy of retinal cells around the optic disc. Some atrophy appears in both normal and glaucomatous eyes but it is more commonly observed in glaucomatous cases. We can observe that an increase in

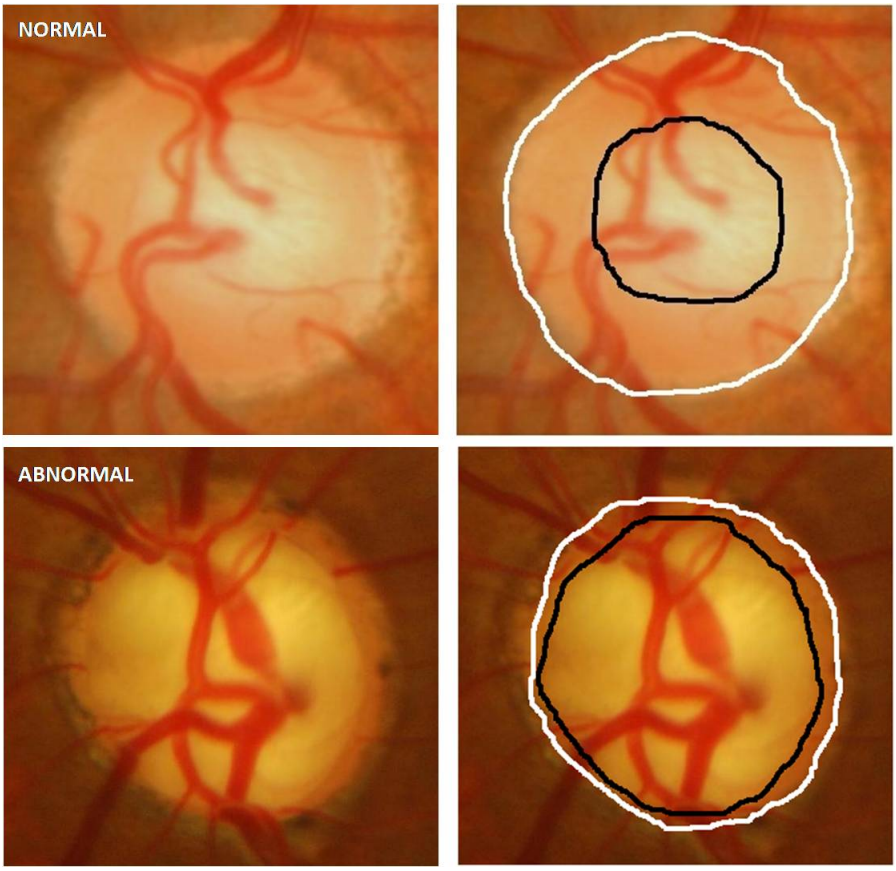

Figure 1.3 Sample normal and Glaucomatous OD depicting the effect of rim thinning due to the disease (left to right). Expert marking in black is used for depicting cup and white for disc boundary.

brightness outside the disc boundary appears in the Peripapillary Atrophy affected pixels in comparison to normal retina. Similar to rim thinning, Peripapillary Atrophy appears as a subtle variation in the disc boundary and it is even difficult for a human observer to differentiate affected regions from normal tissues.

1.1.3 Retinal Nerve Fibre Layer defect

RNFL defect is the most subtle visual indicator of glaucoma in retinal images and occurs due to the loss of the respective layer in retina. It appears roughly as a wedge-shaped region characterized by a loss in brightness in the peri-papillary regions in retinal images (see Fig.1.4(in green)). Visual examination is performed by doctors for typically identifying striations, changes in texture, sudden reduction in brightness and increased clarity of blood vessels.

The subtleness and the difficulty in the identification of these indicators can be seen from Figure.1.5. As can be seen, the cases shown in the figure are very difficult to categorize even through visual inspection, which makes it an elusive task for automated detection. The normal cases in Fig.1.5(a) seem to

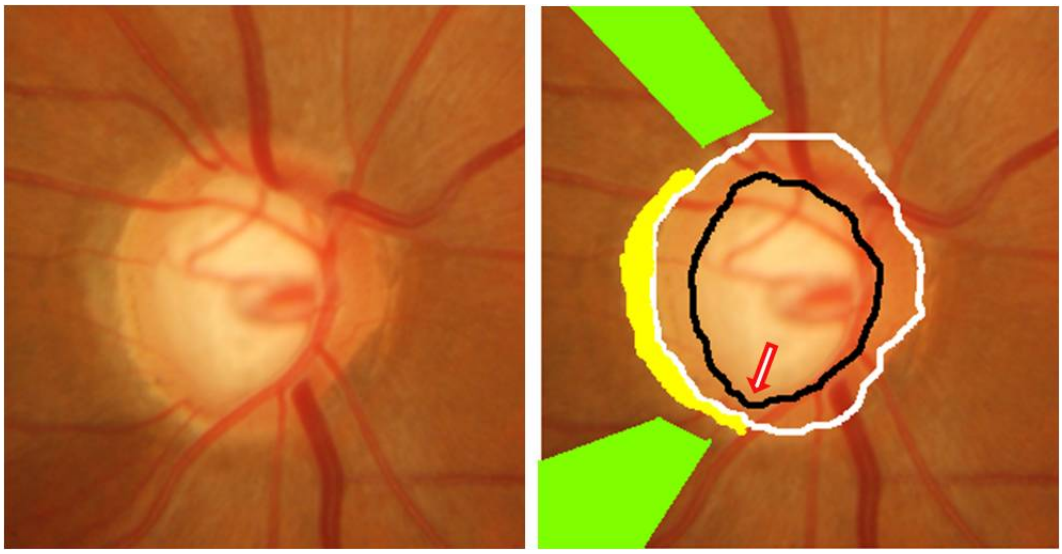

Figure 1.4 Glaucomatous case depicting local rim thinning (indicated by the red arrow), PPA (marked in yellow) and RNFL defect (marked in green).

have similar neuroretinal rim as the confirmed cases in Fig.1.5(b). This is because the intensity is not considered as primary indicator for cup boundary within optic disc. The vessel bends serve as cues for the depth change. Similarly, normal cases and confirmed cases seem to have regions which look alike (refer Figure.1.5) which may be misinterpreted as atrophy or nerve fibre loss defect.

1.2 Previous Works

The problem of automatic glaucoma detection from retinal images has been an active area of research for a decade now [16] [1] [34]. Since, cup deformation within OD region is clinically considered to be the primary and most important of all indicators, much of the literature has focussed on detecting the primary indicator in terms of the ratio of the diameters of the cup and disc (CDR) in the superior-inferior direction. Therefore, detecting cup and disc boundary automatically is a necessary task for automatic glaucoma detection. A significant body of work in retinal image analysis focus on detection and segmentation of optic disc and cup [17] [7].

In contrast to segmentation-based approach, another approach to glaucoma detection has been to use global image features around OD for normal and disease classification [3] [5] [4]. This approach assumes that the morphological changes in OD caused by the disease, can be encoded using the statistical image features, thereby removing the need to identify cup and disc boundaries accurately. Broadly, earlier glaucoma approaches can be categorized as :

Local Approaches : A lot of previous works are there on OD segmentation . The methods range from as simple a technique as thresholding followed by canny edge detector [15] to a more sophisticated

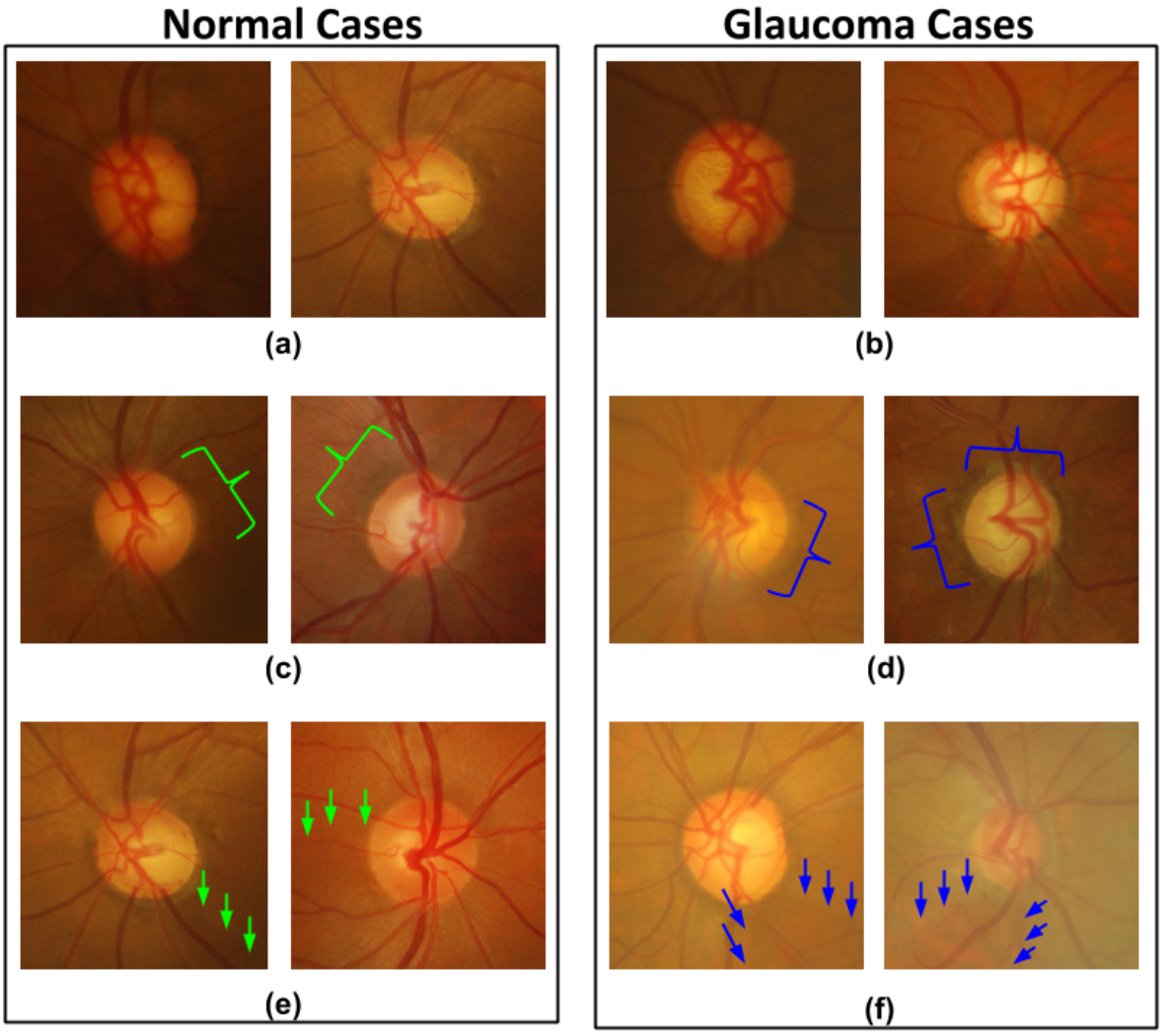

Figure 1.5 Sample images for challenging normal cases in (a)(c)(e) and sample images for confirmed cases due to neuroretinal rim thinning (b), peripapillary atrophy (d) and nerve fibre layer loss (f)

deformable model based technique [16]. Snakes active contour model [26] and morphological methods [33] have also been tried but OD segmentation is typically performed by OD localization, using simple template matching techniques, followed by specifically adapted deformable models [37] [16] for irregular-boundary extraction of OD. Unlike optic disc segmentation, very few methods have been proposed for cup segmentation because optic cup is primarily defined by change of depth which is difficult to detect in a two dimensional image [17] [9].

Cup segmentation has been attempted based on various pixel and superpixel based classification strategies. Recently a superpixel classification based optic cup segmentation technique was proposed for glaucoma detection [34] where each disc image is converted to superpixels over which features are extracted and are classified as cup or non-cup. Similarly pixel level classification where class is assigned

to each pixel based on the feature extracted using numeric properties of the pixel and its surroundings is also used for cup segmentation in [1]. Apart from these, vessel bends and pallor information [35] [36] based information have also been used to provide depth cues for cup segmentation. Based on segmentation of optic disc and cup region, the diagnosis is done by quantifying cupping on the basis of obtained cup-to-disc diameter ratio (CDR) and then applying clinically defined threshold on the CDR value.

Global Approaches : Here, the ROI is represented by a set of features which is later put to classification. Different features have been tried in this direction. A global strategy has been adopted in [5] [3] where raw intensities, Fourier domain features and B-spline coefficients are used to encode morphological changes avoiding explicit segmentation. In [5] [3], preprocessing is required to suppress deviations in global feature characteristics due to structural variations. Thus, supervised classification is performed on various statistical features based on color, intensity and geometry which are computed for each image after segmenting the vessels and inpainting them. Bock et al. [4] presented a different preprocessing solution using polynomial surface fitting operation to normalize large intensity variations in retina followed by vessel suppression. On a test set of hundred images, such pre-processing (before feature extraction) was shown to improve detection of normal cases. However, only a slight improvement in detection of diseased cases was observed.

Similar features with compression using principal component analysis were used for detection of glaucoma in [28] . The major difference was in preprocessing scheme which included three types of corrections : non-uniform illumination correction , size differences normalization for pappila, and blood vessels elimination before extraction of features from the images. Texture features have also been employed for glaucoma detection in [2] where energy distribution over wavelet sub bands is used to compute features. The images are classified based on the energy in the detailed subband. Performance reported is accuracy of 95 percent with testing done only on twenty images. This result cannot be generalised to a large scale screening scenario considering the variability captured in the data set is very less as compared to variability seen across and within class in retinal fundus images.

Apart from these, glaucoma detection have been tried from Confocal Scanning Laser Tomography (CSLT) images in [22] [23] where the obtained 3D optic nerve images were used to derive features using the moment method. In [29], data mining technique have been applied for diagnosis of disease. Some have also tried detecting the disease by combining different examinations like visual field test, IOP (Intraocular Pressure) measurement along with fundus image processing. This is not feasible for large scale screening especially which also aims at reaching remote areas.

The various local and global feature based strategies tried for glaucoma detection are successful in capturing glaucoma only upto a certain extent. To the best of our knowledge only [34] and [5] have reported significant classification results on images as normal or glaucomatous. One is global feature based classification method and other is based on thresholding the CDR. The advantages and limitations of both the approaches is explained in the next section followed by the motivation and summary of our approach.

1.3 Motivation and Proposed Approach

The nature of challenges in automatic detection of glaucoma can be seen in the Figure.1.5 and Figure.1.3. The Figure.1.3 shows normal and glaucomatous optic disc regions of the retinal image with their respective cup boundaries and Figure.1.5 shows sample normal and glaucomatous images. Discriminating between normal and glaucomatous images is very difficult in a two dimensional image as structural details of retina are lost in the projected color fundus image obtained through fundus camera. As a result a lot of inter-class and intra-class variations are observed in glaucoma images. Also, segmentation and identification of these ill-defined boundaries is a difficult task as local intensity based statistics are insufficient to discriminate between OD, cup and neighbouring deformations [16]. In the clinical exam, the three dimensional nature of the cup is used by the experts to detect cupping. Previous works have mainly aimed at local feature based segmentation approaches and global feature based classification approaches. Both the features have inherent advantages in view of the given detection problem but at the same time they also pose some limitations.

In local feature based approach, quantification of glaucoma in terms of enlargement in the cup region depends heavily on the accuracy of segmentation. The results are used to derive vertical CDR. A small segmentation error may lead to significant deviation in CDR from the true value, resulting in erroneous detection of glaucoma.Hence, a CDR based system may not be sufficient given the variability and the challenges in the given disease. The segmentation based methods are quite sensitive to small glaucomatous changes in the optic disc region since, by design, they encode local cup deformations. But it is very difficult to achieve satisfactory segmentation performance of these regions particularly, of the cup region which, in general, is challenging in the absence of three dimensional (depth) structural details.

The second approach based on global statistical image features assumes morphological changes in OD caused by the disease can be encoded using global image features, thereby removing the need to identify cup and disc boundaries accurately. Consequently, limitations of segmentation based techniques of glaucoma detection are eliminated. They rely on a statistical evaluation of the disc region by extracting image-level features for the classification of glaucoma. The method utilizes well known appearance-based classification techniques used in object and face recognition. Both intensity and geometry based features have been exploited under this approach and by designing the features carefully this can robustly encode inter and intra-image variations. This does not require explicit segmentation of the boundaries but these features by design are usually implemented to describe easily identifiable global characteristics in medical images [32]. Therefore there are certain pitfalls in using global image features also for describing certain pathology in medical images.

1. Global image features are insufficient for encoding subtle local deformations in anatomical shape or highly localized change in intensity distribution due to pathology. Such localized change man-

date the use of local image features to identify presence or absence of abnormality at image level [32].

2. It may be possible to encode certain localized pathology using global image features by first applying local filters that enhance intensities in the affected pixels. Such methods also run the risk of encoding intra-class variations in intensity, tissue pigmentation and normal anatomical shape, which is significant in retinal images [11].

3. There is always a risk of adapting image features for a particular image dataset through transformations like Principal Component Analysis. The resultant features may identify global parameters discriminating between the normal and abnormal classes, while failing to encode subtle disease indicators. Suspect glaucoma cases in general are quite close to normals, only exhibiting subtle variations, and hence will be classified as normal.

Any glaucoma detection scheme based solely on local or global has to trade off specificity for sensitivity and vice versa , given the challenge in cup segmentation and variabilities in disc appearance. The focus of previously published work is mainly limited to the independent analysis of local or global features. Only [34] and [5]) have reported classification results on images as normal or glaucomatous. The results in [34] (Figure.1.6) show that the local approach may lead to false detections when pallor is very weak or absent. As mentioned in [34], it may lead to over-estimation of very small cup and under-estimation of very large cup. Similarly, in [5], the sensitivity has been traded off for specificity with sensitivity being 73% and specificity being 85%. This may lead to a sense of false security among the cases who are falsely detected as normal.

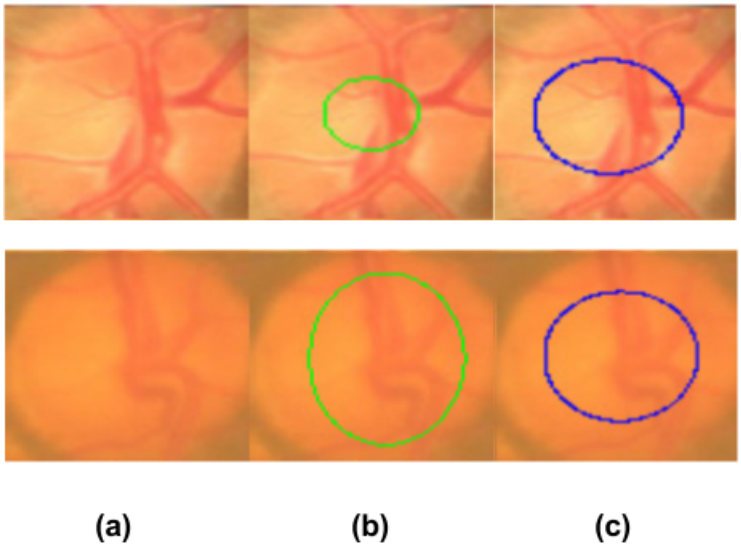

Figure 1.6 (a) Original color fundus image, (b) marking by an expert (in green), (c) result got by [34] (image from [34])

In this thesis, we examine two main questions in the context of glaucoma detection from colour images: what is a good strategy which does not tradeoff specificity for sensitivity or the otherway round? and Will employing the two approaches together lead to a better assessment by overshadowing the limitations posed by two approaches? We propose a new global feature for the detection of glaucoma. It is followed by the experiments conducted to analyse the impact on detection performance in a hierarchical setting as explained in Chapter 3 of this thesis. Chapter 4 consists of a two stage cascade system using global features based detection as first stage and local feature in second stage. The thesis is concluded in Chapter 5 with a detailed discussion.

Chapter 2

Classification with Global Features

Glaucoma affects the optic disc (OD) and surrounding regions in retina which can be observed in color retinal images. Therefore given a retinal image, a region of interest (ROI) of size $M \times M$ centered on the OD is extracted from the input image (Fig.2.1). The green plane is used for all the processing in the first stage as it provides the maximum contrast. The aim here is to identify as many normal cases as possible. Hence, a global representation that accentuates the abnormalities while de-emphasising the variations in normal class is desirable. Such a representation was proposed for detecting bright lesions present in diabetic macular edema in [11]. Here, a transformation known as Generalised Motion Pattern (GMP) was applied to the image after which a Radon transform based feature was extracted for classification. The GMP essentially involves inducing motion to an image to transform the image such that the spatial extent of abnormalities or relevant information within an image is extended, whereas other background (irrelevant) intensities remain unchanged or are attenuated.

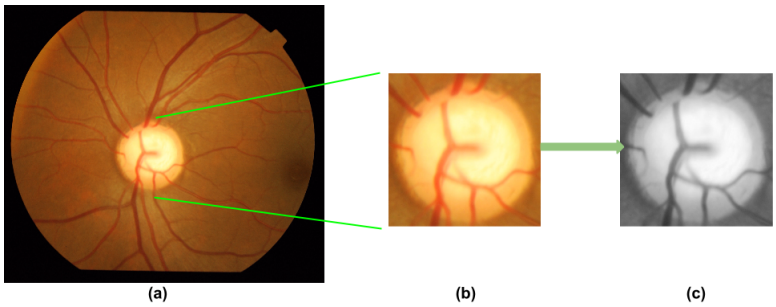

Figure 2.1 (a) Original color fundus image, (b) ROI extracted from original image and (c) green plane of ROI

2.1 GMP for Detecting Bright Lesions

GMP has been proposed and utilized to detect abnormalities, specifically hard exudates which appear as localized bright (lesions) structures in retinal images [10]. Motion serves to spatially spread and thus

accentuate intensities corresponding to high contrast lesions over the normal background. Motion is simulated in a static image by applying a rigid transformation in steps, with origin at the center of the image. The transformation results in generation of several samples at each 2-D location. The sample values (Intensities) at each location are coalesced to generate the desired GMP as shown in Figure.2.2.

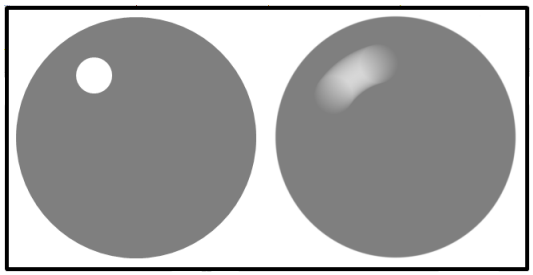

Figure 2.2 Image with simulated bright lesion (left) and corresponding GMP image (right) obtained by inducing rotation in steps of 1° to the extent of $\pm 25^\circ$ to the original image.

Given a region of interest $I(\bar{r})$ with $\bar{r}$ being the position vector, the GMP I_{GMP} is generated as follows:

$$I_{GMP} = S(T(I(\bar{r}))) \tag{2.1}$$

In the discrete case, application of geometric transformation T yields a sequence of transformed images which is combined using the coalescing function S. Further details on GMP generation can be found in [11]

2.2 Image Representation for Glaucoma Detection

We propose to extend the use of GMP to our problem of differentiating between normal and glaucomatous retinal images. A normal optic disc in a colour retinal image is characterised by two low contrast, concentric, roughly- circular structures, the disc and cup. The region between boundaries of these two structures known as the neuroretinal rim is affected due to morphological changes in these two structures. Additional changes due to glaucoma also arise around OD region in the form of subtle variations in intensity and texture as explained earlier in section 1.1. All these changes need to be captured through features used for describing both normal and abnormal (glaucoma) cases. Besides, loss of OD boundary definition is also seen in the presence of these variations and in the absence of 3-D information, cup bpundary is difficult to identify using vessel bends and extrapolate it along with other cues such as subtle change in color. Thus, unlike the bright lesion detection problem in [10], using GMP for glaucoma detection has various challenges:

1. Glaucoma appears as a subtle change in the structure of cup and disc boundary. Consequently, the strategy proposed in [5] namely, using a normal background as a reference and smearing the intensities corresponding to the abnormality to generate a GMP is inadequate. Such a strategy will instead serve to suppress subtle glaucoma indicators like localized rim thinning.

2. It can be observed from Figure.1.5 that the relative contrast of cup and disc is not consistent along the cup boundary for both the normal and abnormal cases. Therefore selection of T and S need to be such as to detect local thinning along the cup boundary while taking care of such inconsistencies.

Coalescing function S: The coalescing function was set to be the pixelwise maximum as it helps preserve perceived intensity difference between cup and disc region and achieve the best separation between various abnormal structures. This choice is also suitable to capture PPA and RNFL defect, if present.

Motion Parameters: Motion parameters needs to be chosen such that it accentuates the structural variation in glaucoma along neuroretinal rim. Four variables namely pivot for motion, type, extent and step size of motion needs to be handled under motion parameters. We have explored rotation, translation and combination of two motions in generating global features for Stage-1. Choosing a single type of motion will not suffice given the variations that needs to be captured. The details about the extent of motion, step size of motion, pivot point and features computed on the obtained motion pattern representations are presented in next subsections.

2.2.1 Translation motion based GMP

In designing the global features, the deformation in the OD region in the superior-inferior (top and bottom) as well as nasal-temporal (left-right) regions are of interest. Thus, horizontal (H) and vertical (V) projection profiles of the ROI are candidates. However, the vessel density in OD region varies across subjects. A translation-based GMP essentially extends the structures in the OD region in the direction of motion. This aids in minimising the vessel-based variations in the derived GMP. Hence, feature extraction is done from the GMPs. The list of designed features are:
(i) projection profiles f_p in H and V directions,
(ii) the variation in the profile f_d and
(iii) profile shape f_c

The translation of an ROI in direction t_θ results in $I_{GMP}(\bar{r}, t_\theta)$. In the discrete case, t_θ is expressed as $T = t_\theta(nt_0)$; $n = -(N-1), .., -1, 0, 1, ..N-1$. It denotes translation of vector t in steps of t_0 in the direction θ with respect to the horizontal. The I_{GMP} thus generated, can be expressed as

$$I_{GMP}(\bar{r}, t_\theta) = \max_n t_\theta(nt_0)(I(\bar{r})) \tag{2.2}$$

For each θ, $2N$ images are generated which are combined by taking a pixelwise maximum. Sample ROIs, the GMPs generated by inducing translation motion and their vertical projections are shown in Fig.2.3. The figure shows both normal and confirmed glaucoma cases. It can be seen that the projection profiles encode information about cup width approximately. In figure, W_n represents cup width of given

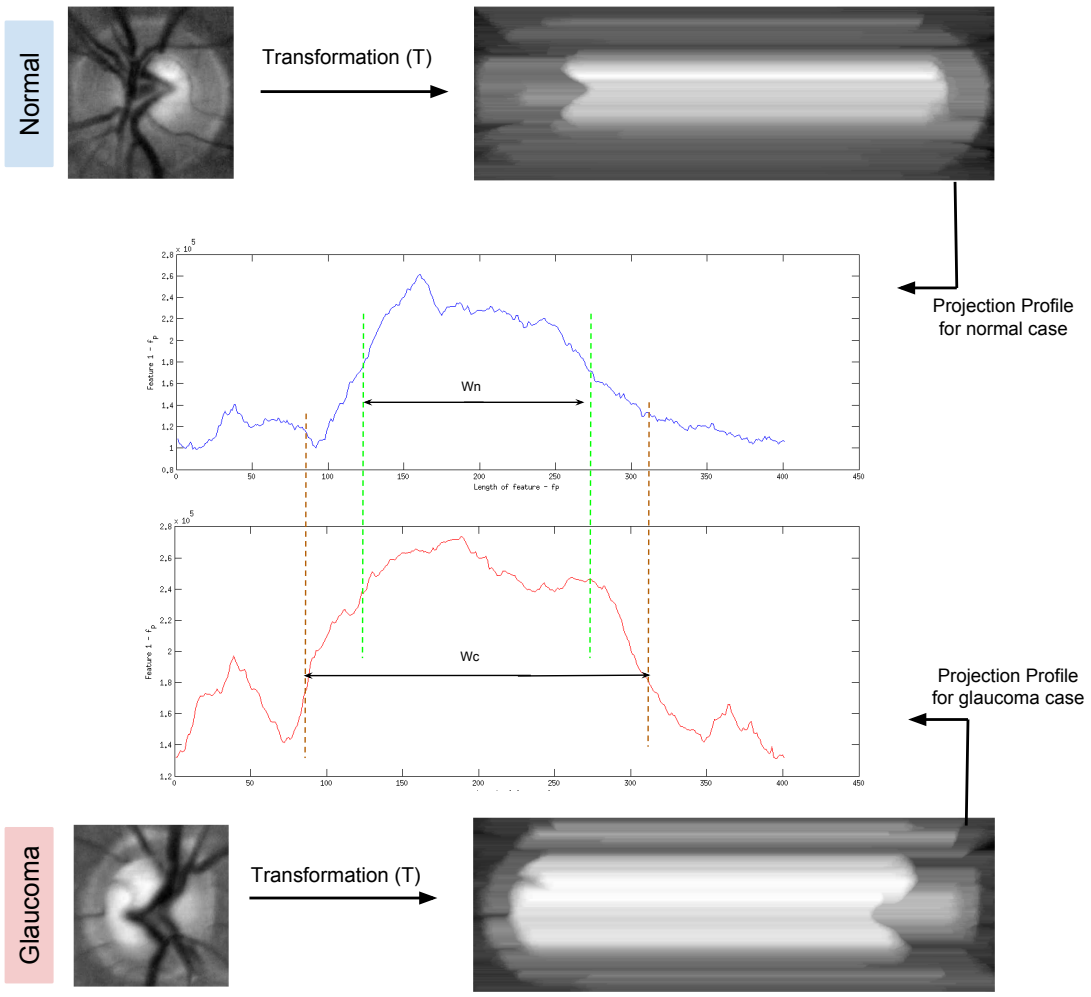

Figure 2.3 Sample Normal and Confirmed Image with corresponding GMP images (obtained by inducing translation to the original image) and the extracted projection profiles.

normal image and W_c represents cup width of glaucomatous case. In the glaucoma case, the cup gets enlarged and hence $W_c > W_n$. A feature vector of length M is derived as follows

$$f_p = P_\theta(I_{GMP}(\bar{r})) \tag{2.3}$$

where P_θ is the projection of GMP in direction θ. Two feature vectors are derived by setting $\theta = 0$ and $\theta = \pi/2$. These are finally concatenated to form the final feature 2M-long vector $f_p(i)$. The concatenated profile is taken to include information about ISNT rule [14]. ISNT rule states that in a normal case, the neuroretinal rim width in the inferior (I), superior (S), nasal (N) and temporal (T) directions should be in a strict increasing order as shown in Figure.2.4. Hence, f_p is formed by joining the two projections.

However, the vertical projection profile is of specific interest as it encodes the cup-disc diameter ratio (CDR) information which is clinically used as the primary indicator of glaucoma. Hence, the following

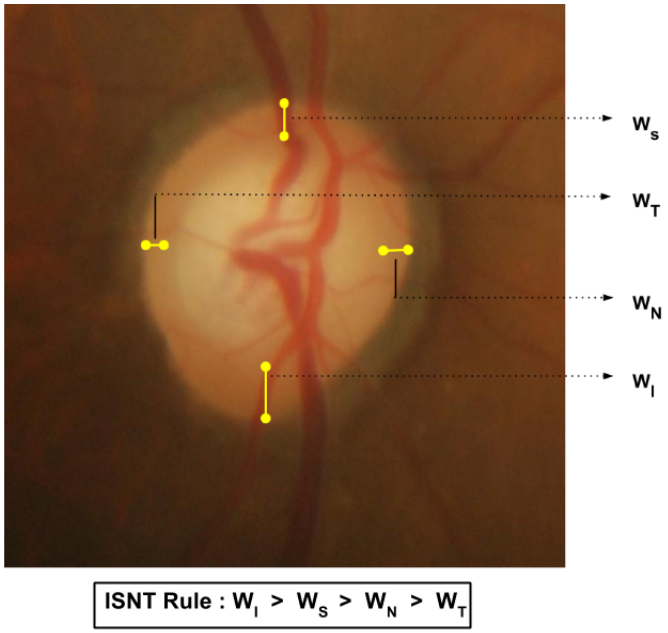

Figure 2.4 Sample image with marked widths of Inferior, Superior, Nasal and Temporal regions as W_I,W_S,W_N and W_T respectively

features are extracted from this profile:
To encode the profile variation, f_d is extracted as

$$f_d(i) = f_p(i+1) - f_p(i); i = 0, .., M-1 \tag{2.4}$$

To encode the shape information, the projection profile is first fitted with Gaussian model and mean level μ is computed. Then the amplitude of the actual profile is encoded by dividing it into L equal levels and for each level,two points t and s are obtained such that $f_p(s) = f_p(t)$. These are taken to construct a vector $f_c(k) = [f_c(s_k); f_c(t_k)]$ where $f_c(s_k) = \mu - s_k; k = L, .., 1, 0$ and $f_c(t_k) = t_k - \mu; k = 0, 1, .., L$. For better perception, the figure 2.5 shows the procedure of encoding shape through f_c.

The primary indicator can be encoded with the help of translation motion but local cupping and PPA etc may not be captured here. Therefore we explored rotation motion based GMP as well.

2.2.2 Rotation motion based GMP

A rotational GMP of the ROI can serve to accentuate the subtle deformation (local notching or global) of the cup and the presence of Atrophy provided the motion parameters are chosen appropriately. We choose multiple pivot points on the periphery of OD and induce rotation motion. This is done to emphasize any asymmetry in the cup-disc morphology. Pivot points $p_i; i = 1, ..8$ were chosen to lie

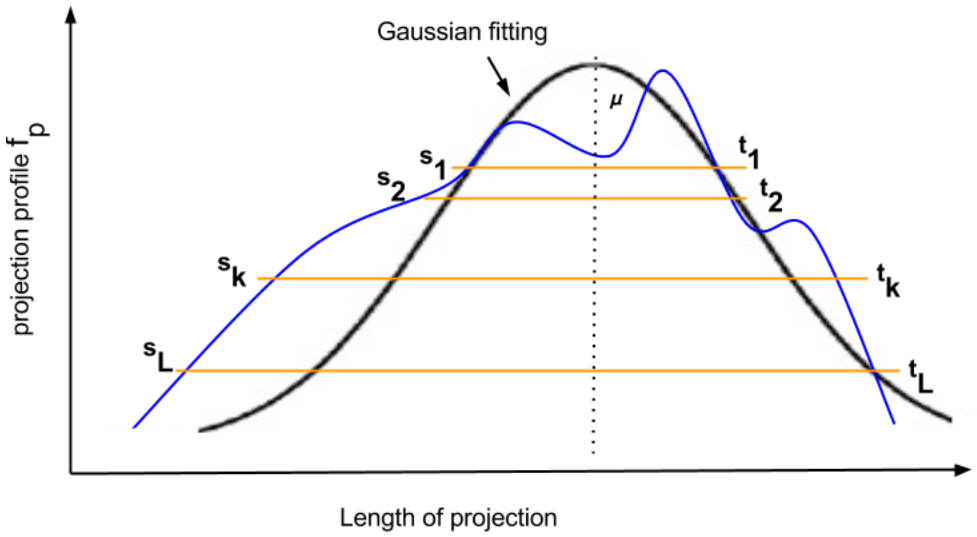

Figure 2.5 Image with synthetic profile showing cuts at k levels along with gaussian fitting to encode shape information

along the best fit circle to the ROI (Fig.2.6). When an image is rotated around a pivot point by angle $\pm\delta$, the information in the sector of width 2δ is accentuated. Changing the pivot location enables capturing information in different sectors. GMPs are extracted by inducing rotation transformation $R_\delta(k\alpha_0)$ where $\alpha_0 = 3^\circ$ is the rotation step, δ was chosen as $15\,\mathrm{deg}$ and $30\,\mathrm{deg}$ for odd and even values of i respectively. It can be represented as $I_{GMP}(\bar{r}, \delta) = R_\delta(k\alpha_0)(I(\bar{r} - \bar{p_i}))$. For a pivot point p_i, a sector with apex at p_i is the relevant part in the GMP. For visualisation purposes, these GMPs are combined and shown in Fig.2.7 as a single image, with all pivots aligned to the centre.

The GMPs are used to extract a second set of feature vector which is constructed from histograms of the eight GMPs. These are rebinned to seven bins and then concatenated to form the final vector f_r. The feature vector for a normal case and glaucomatous case is shown in figure (see figure2.7). The confirmed cases have higher peaks at higher intensities as opposed to normal case. This feature thus successfully encodes the structural distribution of various structures in the ROI.

2.2.3 GMP based on combination of rotation and translation motion

To capture variation of neuroretinal rim thickness along optic disc in all directions, a combination of motions was used. Projections of translated versions of ROI were obtained after applying rotation transformation to the ROI. The process of feature extraction using combination of motion is explained in details with illustrative figure (see Figure 2.8).

Rotation was done in steps of α_o to the extent 0 to δ to generate N rotated versions as shown in Figure 2.8. This is followed by translation in steps of t_o in the direction θ for every rotated image.

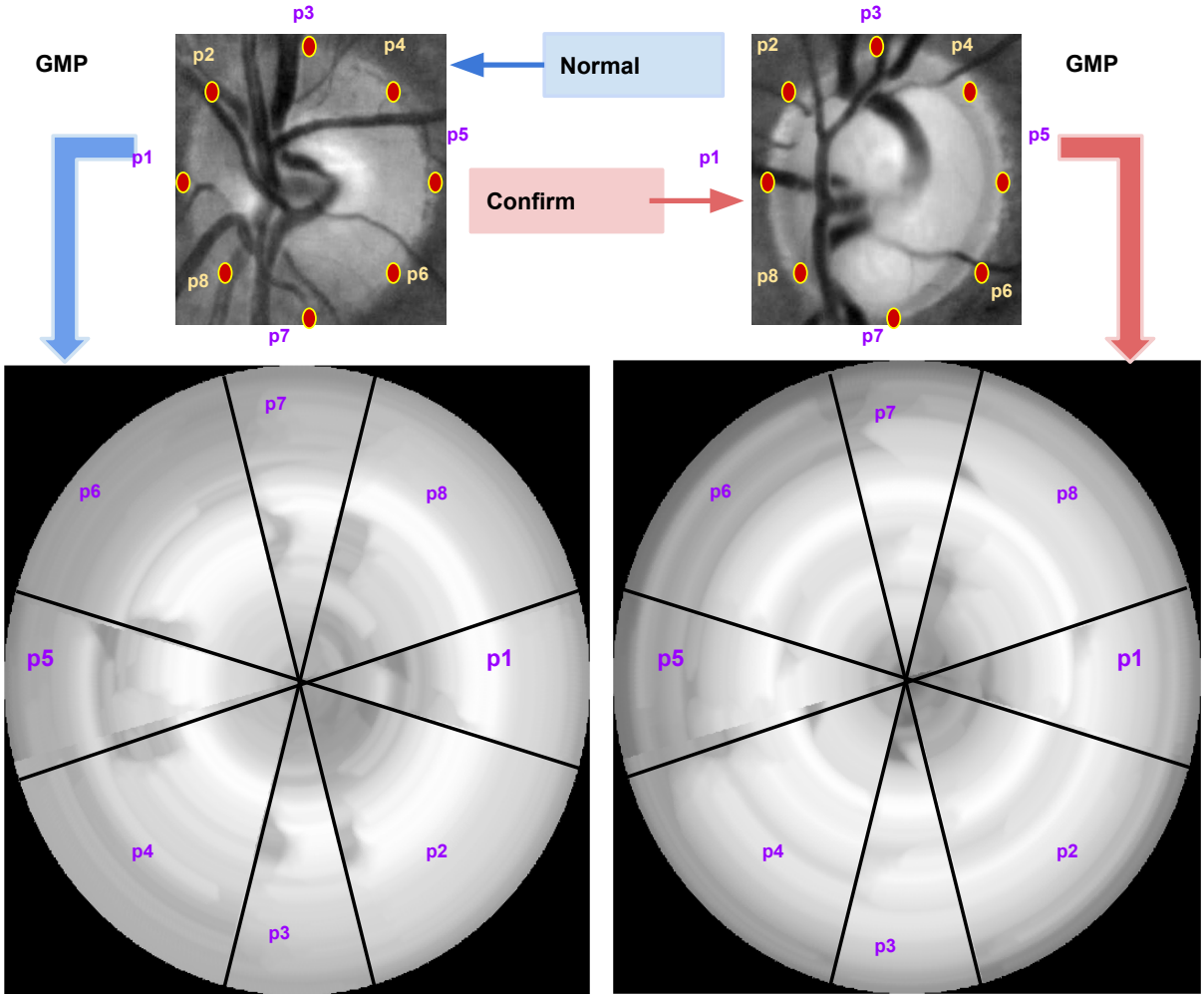

Figure 2.6 Sample images and rotational GMPs with the markings of location of pivot points

Here parameters α_o is chosen to be $3°$, θ is taken to be $0°$ and range of rotation δ is set as $180°$. The projections obtained after each step of applying transformation are stacked on top of each other. To encode variations in the stack of profile, texture feature is computed on stacked projections. Local Binary Pattern(LBP) feature was used for encoding texture information. Mathematically, the feature f_t can be represented as

$$f_t = LBP(P_r(I_{GMPn}(\bar{r}))); n = 0, ...N-1 \tag{2.5}$$

where P_r denotes projections. This is similar to texture of projections(ToP) feature introduced in [24]. Here I_{GMPn} represents projections obtained from every GMP (obtained at each rotated version with α_o step). Here, $I_{GMPn}(\bar{r})$ is represented by following equation

$$I_{GMPn}(\bar{r}) = \max_n t_{\theta\delta}(n \times \alpha_0 \times t_0)(I(\bar{r})); n = 0, ...N-1; \tag{2.6}$$

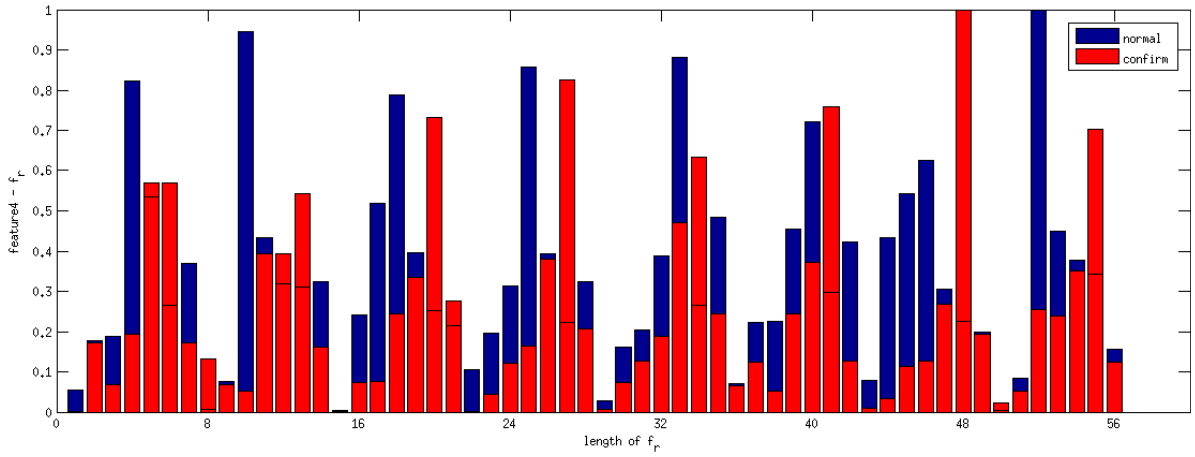

Figure 2.7 Extracted feature f_r for the normal(blue) and glaucomatous(red) case

2.3 Classification

The five features (f_p,f_d,f_c,f_r,f_t) extracted in Stage-1 capture different information. They are combined using a two-step process for getting final classification information of Stage-1: Each feature is classified with a Support Vector Machine (SVM) with polynomial kernel of order three from LIBSVM [6]. The optimal parameters were found empirically for each feature separately. The output of these five classifiers were concatenated as $f_1 = [o_1, o_2, o_3, o_4, o_5]$. This f_1 is classified using an ensemble of decision trees. Decision trees permit diversified decision boundaries which is appropriate for the problem at hand given the underlying challenges.

A set of scatter plots were generated by projecting the features along their 2 principal components (Fig. 2.9). These indicate how the different constructed features cluster the normal (blue) and glaucoma cases. The top two plots and middle (left) plot are for features derived from translation-based GMP while the right plot in the middle row is for the rotation-based GMP. The clusters are tighter for the latter case, though there is overlap between the two classes. Combination of feature reduces this overlap (bottom row, right).

2.4 Experiments and Results

2.4.1 Dataset Details

An annotated dataset of color retinal images consisting of 1845 eye images was collected from a glaucoma center in a local hospital out of which 1272 were labelled as normal and 573 glaucomatous, based on the majority opinion of 3 glaucoma experts. The size of each image is 1494x1996 pixels. Ground truth for the dataset was collected from 3 experts with image level annotation as normal, suspect and confirm case of glaucoma. A gold standard for the expert annotation was found using a majority

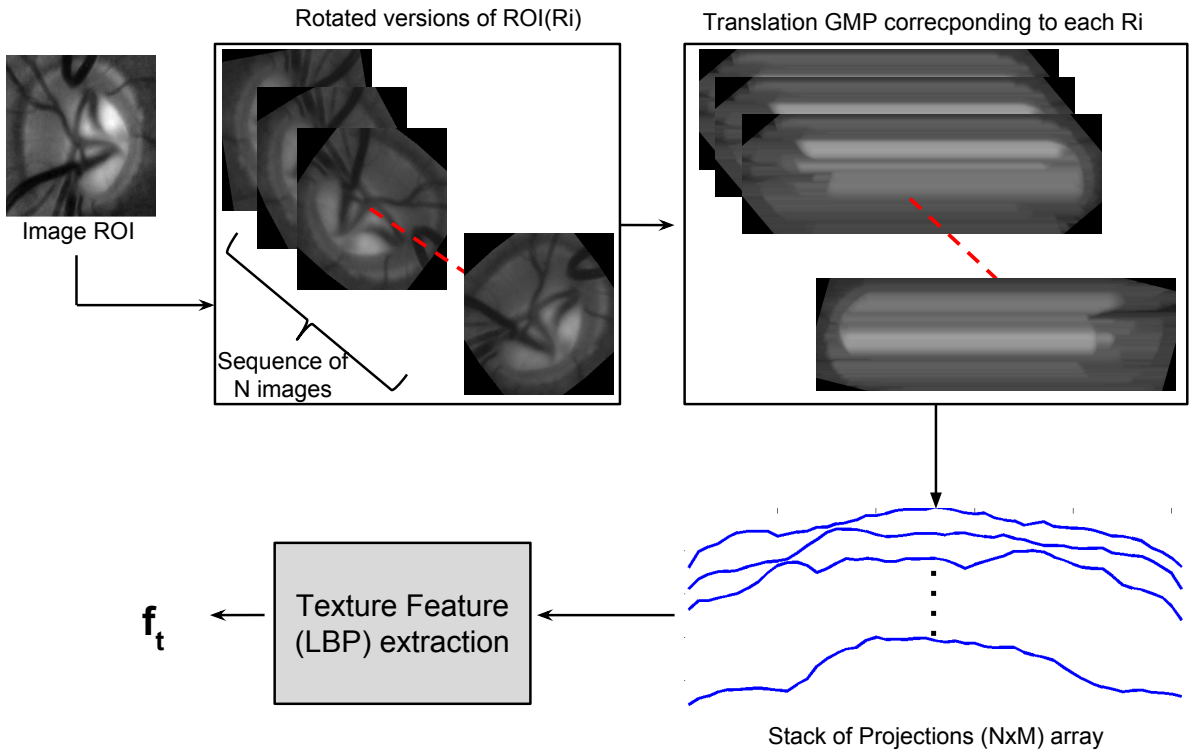

Figure 2.8 General flow for extraction of features through combination of motion applied to Region of Interest

voting on the decision by experts. Cases where no consensus could be found were removed from experiments and suspect category was combined with confirm class. The performance of this stage (Stage-1) is evaluated using this dataset + 800 images (used as training set).

2.4.2 Evaluation Scheme

All ROIs are resized to 401×401 pixels. All processing was restricted to a circular region extracted from a resized ROI with a mask of radius 200 pixels.

The performance of the system was assessed at various levels against the ground truth using receiver operating characteristic (ROC) curve analysis. The area under the ROC curve (AUC), sensitivity (SN) and specificty (SP) were used as global metrics. The first set of experiments evaluated Stage-1. Five variants were evaluated to assess the contribution of each feature towards classification performance of Stage-1. The variants were generated by combining features one by one, with the i^{th} variant generated by concatenating first i features proposed in Stage-1. The performance comparison of all these variants is done using ROC curves obtained by applying different thresholds on the probabilistic output from ensemble of decision trees.

2.4.3 Results

ROC plots corresponding to different variants (explained in Sec.4.3.2) of Stage-1 are presented in Fig. 2.10). It can be observed that the variant1 (black) which uses only f_p based on translation-based GMP, is weakest while the variant-4 which also includes features derived from rotation-based GMP, is stronger in performance. This is due to the fact while the former mostly captures deformation in vertical direction, the latter captures sectorwise-deformation which is useful in overcoming ambiguities in the former. The variant 5 is the strongest due to the fact that it encodes variation in rim in all directions approximately. The AUC for these plots are presented in Table 2.1. Included are the AUC for classification with individual features, for reference. These results underscore the benefit of combining features.

Individual feature	f_{proj}	f_{der}	f_{cut}	f_{rot}	f_{top}
AUC	0.6959	0.6939	0.6670	0.6824	0.6626
Combined features	variant1	variant2	variant3	variant4	variant5
AUC	0.6959	0.7043	0.7713	0.7981	0.81

Table 2.1 Performance figures for Stage-1 on testset

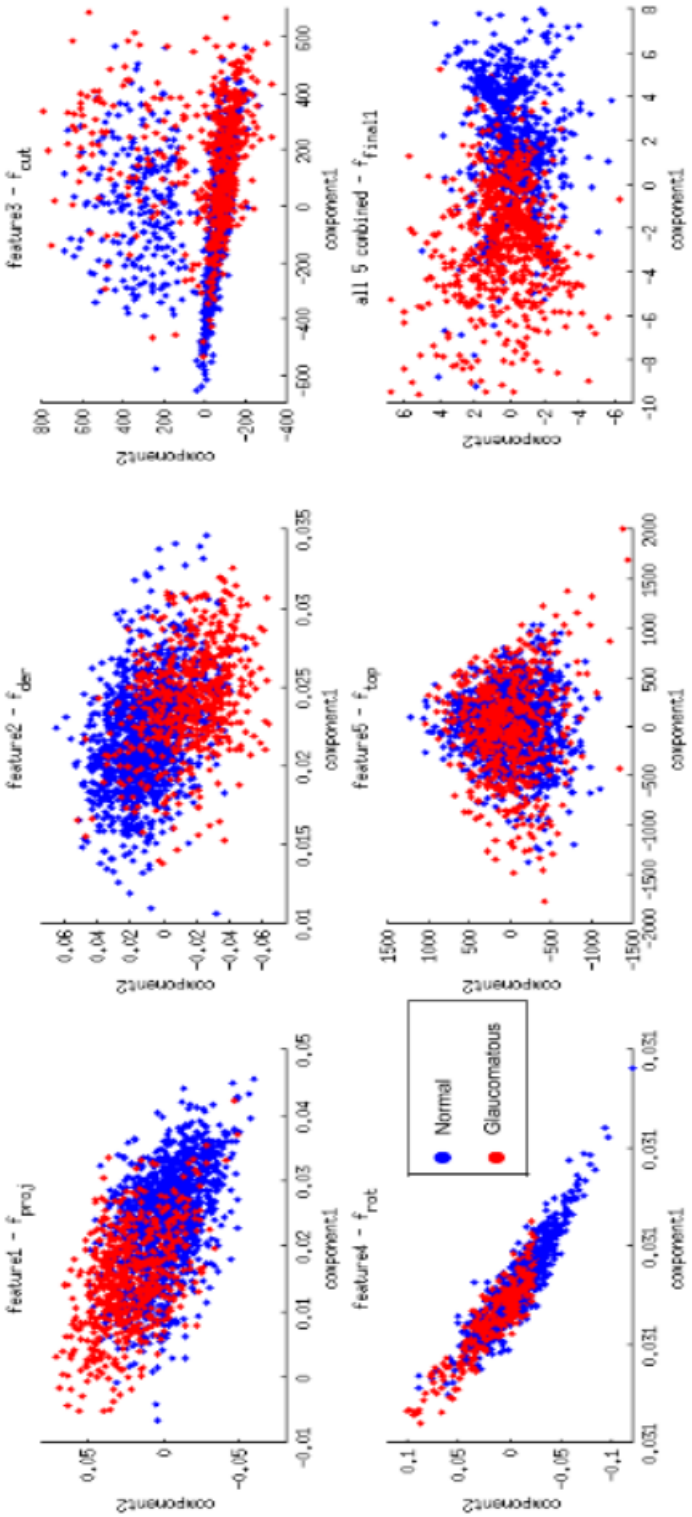

Figure 2.9 Scatter plots for features used in the Stage-1. Top: translation-based; Bottom: rotation based and combined feature.

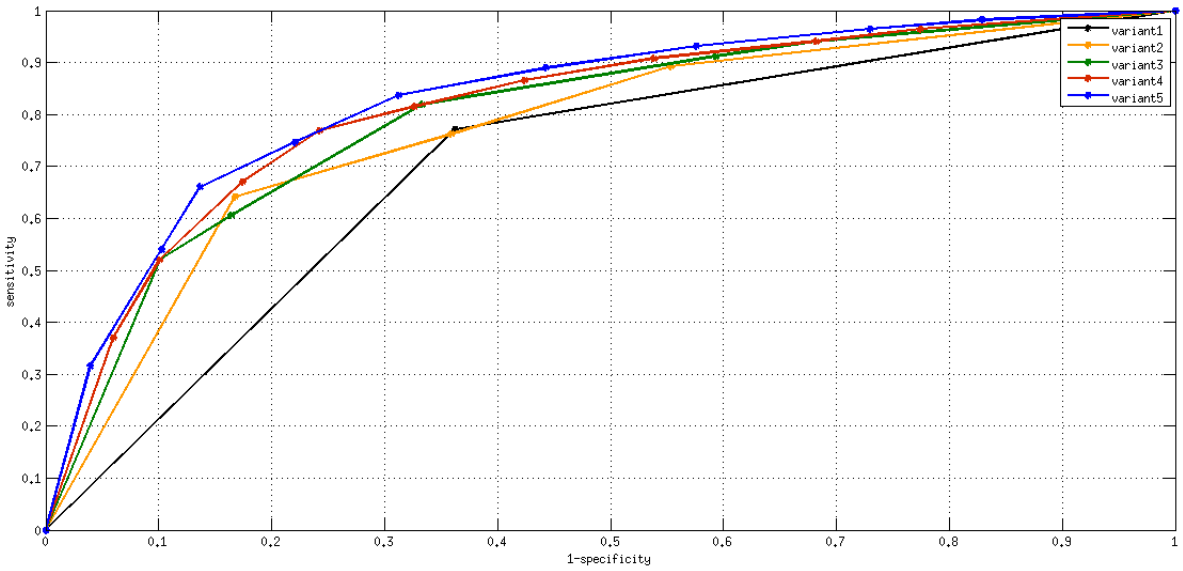

Figure 2.10 ROC plots for Stage-1

Chapter 3

Two stage global feature based classification

In the previous chapter, GMP was used to capture all the indicators of glaucoma with major focus on the primary indicator (deformation). The next study is aimed at extending the ability of GMP to classify secondary visual indicators of glaucoma. Only few attempts have been made towards detecting PPA to the best of our knowledge. First work was reported on Heidelberg retina angiography images [19] by modeling the PPA as a bright contrasting region and localising it using active contours. In colour fundus/retinal images, PPA detection has been done using dissimilarity measure of regions adjoining optic disc [18] and bioligically inspired feature [8]. Detection using texture analysis was also proposed in [25] but the testing was done on a very small set of 26 images. The previous works are largely based on local feature based detection. PPA detection strategy has, so far, not been attempted with a global approach.

The next section presents the details of our proposed motion pattern based feature and experimental results section. The chapter is concluded by presenting a cascade system of features proposed in previous chapter and this chapter for the detection of glaucoma. The work is summarized and concluded in the last section.

3.1 GMP based features for secondary visual indicator (Atrophy)

3.1.1 Proposed features

This feature aims at capturing perceived intensity difference in the regions adjoining optic disc. Since PPA commonly appears adjacent to the annular (optic disc) region, the transformation should aim at accentuating intensities corresponding to PPA which appears as bright blob like structure. The given image is segmented into 18 sectors with 20° angle subtended at the center and PPA detection is performed on these regions separately as done in [18]. In [18], statistical features like maximum, minimum, average and standard deviation are computed on two annular patches taken in this sector and dissimilarity is computed by taking the vector difference between the two features. The proposed feature extraction process is explained clearly in the illustration in Figure 3.1

	Sensitivity	Specificity	Accuracy
[18]	0.82	0.72	0.78
Proposed	0.812	0.57	0.687

Table 3.1 Performance figures for Proposed PPA detection and for [18]

For each sector Figure 3.1(b), rotation motion with step size α_o and pivot at the center was used to generate sequence of N images with maximum coalescing function. The histogram of the GMP is computed(as in Figure 3.1(c) for every annual sector of width 40 pixels starting from center of the image as the location of intensities also matter for Atrophy detection. Histogram of each annular sector will provide information about how intensity distribution is varying in the regions within and adjoining OD regions. The cup and PPA information will not be fused together as may be the case in the combined histogram.

3.1.2 Experiments,Results and Validation

A dataset consisting of 55 training images and 59 test images was used in this study. Each image was divided into 18 patches giving 990 and 1062 region of interest for training and testing respectively. The classification using proposed features was done using ensemble of decision trees and were evaluated using sensitivity, specificity and accuracy values. The results were also compared against [18]. These are tabulated in Table 3.1.

The results show that the proposed feature achieves similar sensitivity as [18] but at the cost of low specificity. However, the global features based detection of Atrophy have shown promising results and need to be improved further. The feature extracted here is the most naive feature which could be extracted from the obtained motion pattern images. Encoding the information present in motion pattern images with different features may help in raising the bar of specificity.

3.2 Hierarchical system

This section includes experiment conducted to analyse if a cascaded system helps in improving detection performance using global features. The first stage includes concatenated global feature from the first chapter. The threshold in classification at this stage is taken in a way that it retains almost all malignant cases. It tends to have lesser false negatives or higher sensitivity and lower specificity. The second stage with the global features for atrophy is added with input as the images left after the classification in stage 1. The following subsections presents the details of dataset and obtained results with this hierarchical system.

	Sensitivity	Specificity	Accuracy
Proposed PPA	0.812	0.57	0.687
Cascade System	0.817	0.65	0.73

Table 3.2 Performance figures for Hierarchical System and Proposed PPA detection

3.2.1 Dataset

The images (1040) left after classification of Stage 1 is passed through the ppa stage (Stage-2). The training for Stage-2 is done using 114 images used for our experiments in previous section. Sensitivity, specificity and accuracy is calculated to see if the cascade helps in improving the result got through PPA detection above. The following section contains the table and concluding remarks.

3.2.2 Results

The classification using proposed features was done using ensemble of decision trees. These are tabulated in Table 3.2.

The results show that the system achieves similar sensitivity but helps in raising the bar of specificity. This stage may help us to remove 1/10th of total images which needs to be passed on to the next level if we cascade further.

3.3 Conclusion

The cascade also does not perform well in terms of specificity values. Hence, the stage 2 PPA detection will be based on the method given in [18]. Also next chapter will be more focussed on evaluation of hierarchical system using both local and global approach based features than on details of stage 2 as this stage has been borrowed from previous works. The aim of this thesis is (i) to study the effects of cascading two different type of approahes ; (ii) to see if we can prevent the trade off between sensitivity and specificity that happens with independent analysis of the two approaches.

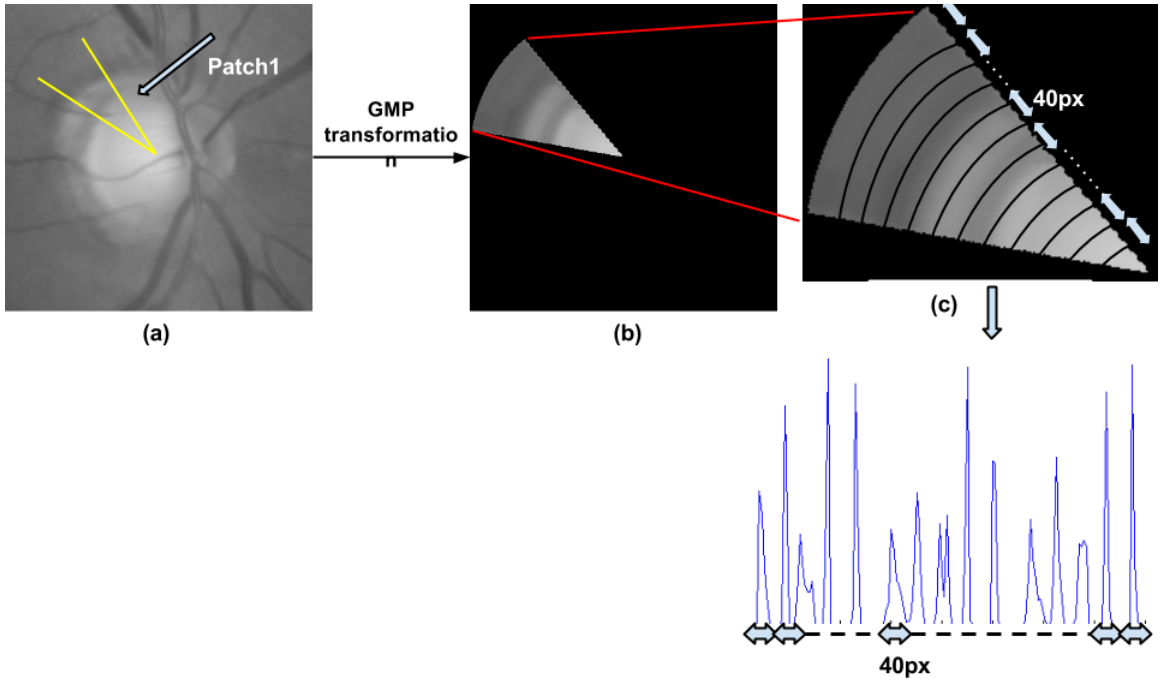

Figure 3.1 (a) Original Image, (b) one out of 18 sector is taken and GMP representation is obtained, (c) GMP is divided into annular regions of 40 pixels width, (bottom) concatenated feature extracted from each annular region

Chapter 4

Hierarchical System using global and local features

This chapter gives the details of stage 2 used in hierarchical system using local approach based detection of glaucoma proposed in [16] and [18] in stage 2. Since the aim was to test cascade type of system for minimising the trade-off that happens between sensitivity and specificity, Stage 2 is borrowed from Gopal et. al. [16] [18]. This is followed by the final system design. So far, to the best of our knowledge, no attempts have been reported to assess glaucoma using the capabilities of both the approaches (local and global) to achieve better and satisfactory diagnosis. This thesis presents a hierarchical approach to effectively address the limitations presented by earlier approaches.

We have taken a cascade design for glaucoma detection as it offers flexibility in setting different goals for the two stages: Removal of as many true negatives (normals) as possible in the first stage; detection of as many true positives (glaucoma cases) as possible in the second stage. Lowering the number of normals passed by the first stage should aid in designing the second stage for high overall sensitivity without compromising the specificity. We present a design with a first stage based on global features and a second stage based on local features for classification. Global features are likely to be less sensitive to local deformations since both the normal and glaucoma classes present a subtle difference in terms of OD appearance and morphology. Hence, a comprehensive set of local features which are sensitive to OD changes, at different scales, are employed in the second stage. In the coming section, details of this stage are provided followed by the description of the experimental setup used and obtained results.

4.1 Stage2 - Classification with Local Features

Stage-2 is aimed at detecting multiple indicators (CDR, atrophy and RNFL) which requires local approaches. Here, the indicators are independently detected and based on the outcomes of individual indicator detection or quantification, the final feature vector is constructed.

4.1.1 Feature Extraction

The methods used for OD and cup segmentation and the quantification of CDR were those reported in [16]. Atrophy and RNFL defect detection was done using methods adopted from [18]. The statistical distribution of different local image structures such as vessels, edges, pallor etc. within the segmented OD and cup region can also give more relevant information about OD deformations. Hence, we used the representation (f_{st}) propsed by same authors which they derive using a method in [27] where a filter-bank of size l consisting of first order Gaussian derivative filters at different scales was used to derive a response vector of length l which were clustered using k-means clustering, with k representing the number of different retinal image structures. $k = 7$ was found to best represent different structural profiles within the OD region. In that work, for a test image, an image point is assigned to one of k-clusters based on the distance of the l-length response vector computed for the point to the cluster.

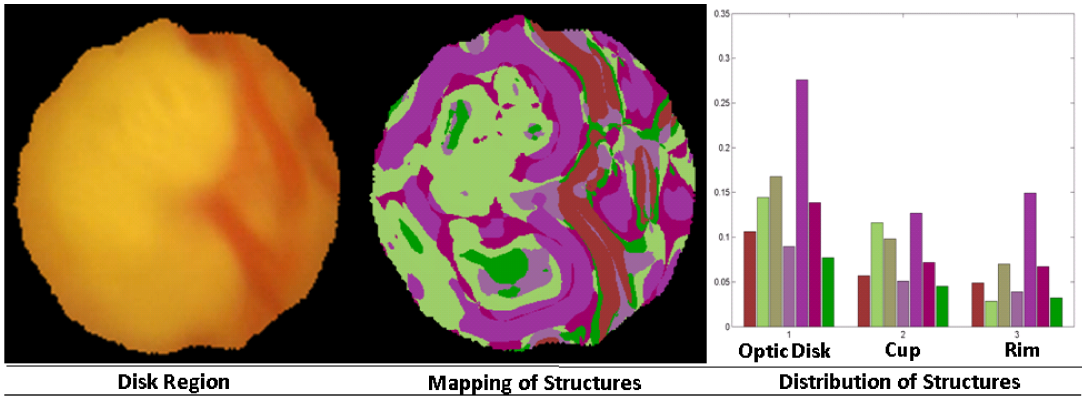

Figure 4.1 Relative distribution of structures within a sample OD region.

Fig.4.1 (second column) depicts mapping of each image point of the sample image to one of the 7 colour coded clusters. In order to minimize the effect of inter-image intensity variations on the clustering step, f_{st} is extracted from the given green color channel and its two normalized versions. Since the amount of glaucomatous damage is determined by the extent of rim and pallor regions, a reference image is chosen from the normal and glaucoma class. Matching the histogram of the original image with 2 reference images to derive the normalised versions, serves to enhance the rim and pallor region, respectively. Finally to capture the symmetry of the OD region the difference in f_{st} computed for regions above and below a line that bisects the OD region (horizontal) is included as asymmetry is an indicator of glaucoma. The final set of features derived from Stage-2 are:

1. Cup-to-disk vertical diameter ratio: x_{cdr}. This ratio lies in the range of [0-1].
2. Cup-to-disk area ratio: x_{car}. This ratio lies in the range of [0-1].
3. Atrophy presence decision: x_a^{inf} and x_a^{sup} in the inferior and superior directions, respectively.
4. RNFL presence decision: x_{rnfl}^{inf} and x_{rnfl}^{sup} in the inferior and superior directions, respectively.

5. Relative distributions of image structures: $3 \times 7 \times 3 = 63$ features within *ONH* region.

6. Symmetry features $7 \times 3 = 21$.

4.1.2 Classification

The classification in Stage-2 is done using an ensemble of decision trees for the same reason explained in Section.2.3. This stage aims to capture subtle local changes, a structurally unstable classifier is best suitable for classification as it would help in capturing small perturbations in the feature vector.

4.2 Final system using hierarchical classification

The final cascaded system is shown in (Fig.4.2). The system was implemented by training both the stages on a common set of 800 images (329 normal and 471 glaucomatous) as well as different training sets. In the latter approach, the second stage was retrained using images left out after the classfication through Stage 1. The Figure.4.2 shows general flow of the final hierarchical system.

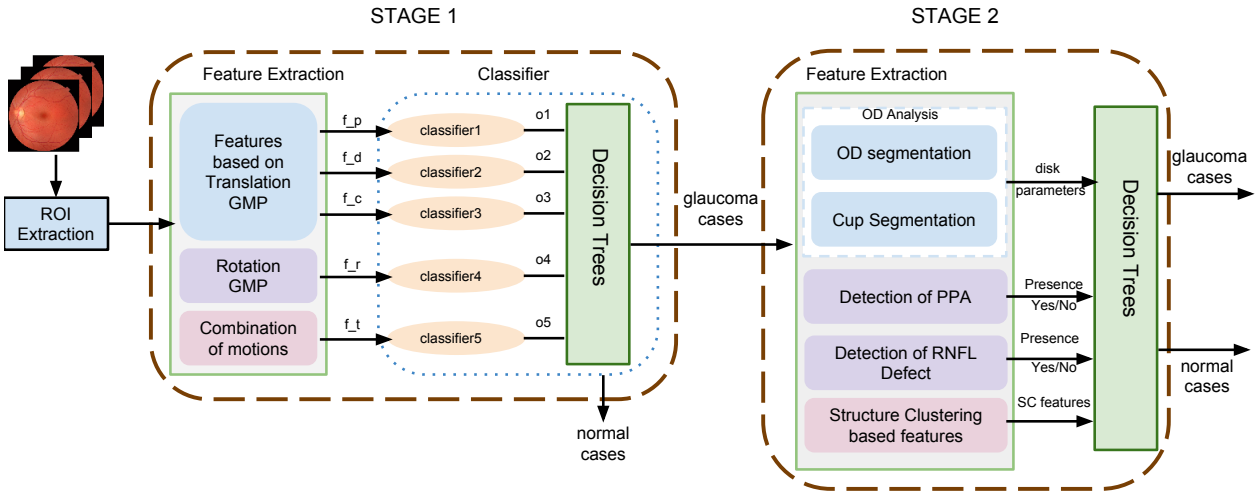

Figure 4.2 Block diagram of the proposed glaucoma detection system

4.3 Experiments and Results

4.3.1 Dataset Details

A total of 1040 eye images was passed from first stage out of which 585 were labelled as normal and 455 glaucomatous. This stage is evaluated using this data. A second set of data was collected consisting of 800 images (apart from the 800 images in training set of stage 1) out of which 652 are normal cases

and 148 are (suspect+confirm) cases. This dataset is combined with 1040 images for testing the system performance after retraining the second stage from the remaining images of stage 1 as mentioned earlier.

4.3.2 Evaluation Scheme

All ROIs are resized to 401×401 pixels. All processing was restricted to a circular region extracted from a resized ROI with a mask of radius 200 pixels.

The performance of the system was assessed at various levels against the ground truth using receiver operating characteristic (ROC) curve analysis. The area under the ROC curve (AUC), sensitivity (SN) and specificty (SP) were used as global metrics.

In Stage-2, detection results of multiple indicators are included as it performs better than detection using only CDR.For comparison purposes, two CDR based systems were implemented using methods in [5] and [34]. As the latter mainly reported a supervised superpixel based method for optic cup segmentation, the OD boundary found in Stage-2 was used to compute the CDR. A separate set of 101 images with ground truth markings for the cup was sourced and used for training in implementing [34]. The two systems were tested on the 1040 eye images.
The hierarchical system was evaluated with the variant five for Stage-1.

In another set of experiments, the effectiveness of hierarchy is analysed by seeing the combined performance of both systems against local feature based approach of stage 2 as it happens to be the state of the art for glaucoma detection. All the performance curves and tables are presented in experimental results section.

Finally the last set of experiments were done to see the effect on performance of combined system when a bigger dataset is dealt and effect of not using same training set for both the stages.

4.3.3 Results

The ROC plots for the Stage-2 (blue) and the hierarchical system (red) (shown in fig 4.3.3) indicate the hierarchical system to be superior in performance. SN, SP and AUC are listed in Table 4.1 for different glaucoma detection systems. In terms of SN and SP, the CDR-based systems ([5] and [34] and Stage-2 with CDR-based classification (row 3)), perform the poorest. It is noteworthy that the SP figures are less than 0.5. The *Stage-2 multifactorial* uses the full set of 6 features performs better than the CDR-based systems. This indicates that including information about secondary indicators helps in significantly boosting the SP value. The hierarchical system has the highest performance. There is a significant boost to SP (23%) compared to SN (3%). This is because the addition of the Stage-1 can mainly help minimise the false positives (normals) in the final output. In terms of AUC, the figures are comparable for Stage-1 (0.81), Stage-2 (0.80) and the hierarchical system (0.835).

Furthermore, the results shown in above table for hierarchical system is with respect to dataset consisting of 1040 images and both the stages are trained using same set of 800 images as mentioned in Section 3.2. Ideally the second stage should be retrained using the images left after stage 1. The perfor-

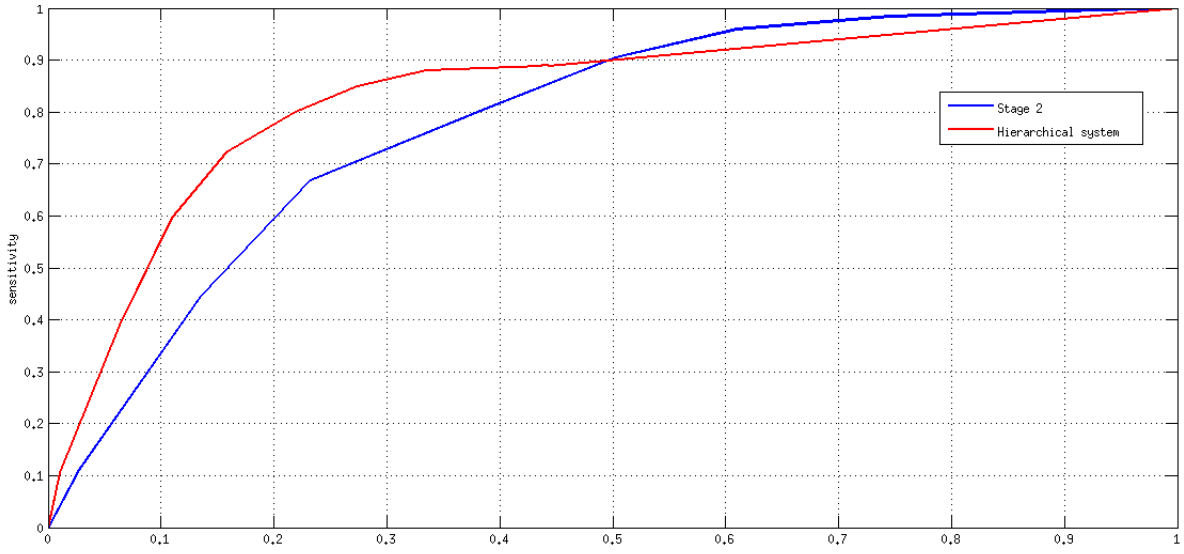

Figure 4.3 Stage-2 and hierarchical system

	Sensitivity	Specificity	AUC
[34]	0.65	0.44	0.558
[5]	0.70	0.46	0.615
Stage-2 CDR	0.70	0.48	0.636
Stage-2 multifactorial	0.79	0.62	0.8012
Hierarchical System	0.8128	0.7658	0.8353

Table 4.1 Performance figures for Stage-2 and hierarchical system and for [34] and [5].

	Sensitivity	Specificity	AUC
Hierarchical System	0.801	0.734	0.8123
Hierarchical System(retrained)	0.8539	0.7935	0.844

Table 4.2 Performance figures for hierarchical system with and without training

mance with retraining was tested with (1040 + 800 + 800) images. The reason to include more images is that the with the previous set the no of normals left after first stage are very less. The second stage can not be trained using those few cases. The performance on the large dataset with and without retraining is given in Table.4.2

Chapter 5

Conclusions

The study was set out to explore automatic detection of glaucoma. The cure for glaucoma is possible only if it is detected in early stages. Thus, the screening of population needs to be done. In a country like India, where the population is growing very fast and technical manpower is in scarcity, the automatic detection will help in reducing pressure on the ophthalmology labs. The present literature has focussed on either local or global feature based approaches. No efforts have been made to integrate the strengths of both the approaches. In this thesis, we try to find answers to two questions related to automatic glaucoma assessment namely, what would be an appropriate strategy, whether combining features in a cascading manner helps improving the performance and whether it should be based on global or local approach alone, as prevalent in literature. The main findings are chapter specific and were summarized within the respective chapters. In this section, the whole work is summarized and concluded with the new directions that can be taken up for further research.

A hierarchical design was posited to be the best to avoid a trade off between SN and SP. Although a cascade of global features has also been tried, yet the hierarchical system with global and local analysis for the first and second stages, respectively, performed the best on a large dataset of 1845 images. This was achieved mainly by controlling the number of true negatives (normals) being passed on by the first to the second stage. The second stage included detection of primary (CDR) *and* secondary glaucoma indicators (Atrophy, RNFL) along with symmetry of the OD region. The superior performance of this stage over CDR-based classification, underscores the importance of expanding the scope of analysis to multiple factors in glaucoma assessment. This naturally incurs additional computational cost which may not be a major deterrent in screening applications. Alternate ways to design Stage-2 (which ensure high SN) can be explored if computational cost is a concern.

The hierarchical design using global features was shown to improve the performance as compared to the results of the second stage alone. This helps in concluding that reducing the number of normals passing through one stage to another improves the performance at subsequent stages. It also extends the areas where the technique of generalised motion pattern can be applied, which opens up the possibilities

that it can be used for various other difficult medical problems apart from glaucoma and mammography and diabetic retinopathy (as given in literature). This thesis will help in the designing of a suitable application which enables the screening process to be carried on a large scale. It should also be noted that given the variability in the data captured in screening scenarios, the parameters may need to be constantly trained upon for the system to give desired results.

Although the thesis offers an evaluative perspective and promising results, there are certain areas still open to further research. Exploring the following areas in the future can facilitate the attainment of the goal of very large scale screening scenarios efficiently.

- More features, which capture RNFL more efficiently using a global feature based approach, can be added in the Stage-1 or as the third stage. The RNFL detection performance presented in the related literature has not been great owing to its subtleness in the color fundus image. Tapping this potential will provide scope for vast improvements in detection performance of glaucoma as well.
- Automatic parameter detection for the generation of GMP for the problem at hand. It will immensely help to capture the variability as and when screening data on a population is collected and examined. This would be a major step towards generalising the whole detection problem.
- Reducing the computation time for the whole process as there is room for optimisation.

Finally, the thesis can be concluded by saying that the hierarchical system really helps in boosting up the overall detection performance. The system is able to capture the strengths of both the approaches namely, local and global.

Submitted Papers

- K Sai Deepak*, Madhulika Jain, Gopal Datt Joshi, Jayanthi Sivaswamy, "Motion pattern-based image features for glaucoma detection from retinal images", in Proceedings of the Indian Conference on Vision, Graphics and Image Processing 2012
- Madhulika Jain, Arunava Chakravarty, Gopal Datt Joshi and Jayanthi Sivaswamy, "A Hierarchical and Multifactorial System Design for detection of Glaucoma from Color Fundus Images", in Medical Image Computing and Computer Assisted Intervention 2014 (Not Accepted)

Bibliography

[1] M. Abramoff, W. Alward, E. Greenlee, L. Shubha, C. Kim, J. Fingert, and Y. Kwon. Automated segmentation of the optic disc from stereo color photographs using physiologically plausible features. *Investigative opthalmology and Visual Science*, pages 1665–1673, 2007.

[2] N. Annu and J. Justin. Automated classification of glaucoma images by wavelet energy features. *International Journal of Engineering and Technology*, 2013.

[3] R. Bock, J. Meier, L. Nyl, G. Michelson, and J. Hornegger. Classifying glaucoma with image-based features from fundus photographs. *Lecture Notes in Computer Science*, 4713:355–364, 2007.

[4] R. Bock, J. Meier, L. Nyl, G. Michelson, and J. Hornegger. Effects of preprocessing eye fundus images on appearance based glaucoma classification. *Computer Analysis of Images and Patterns*, 4673:165–172, 2007.

[5] R. Bock, J. Meier, L. G. Nyl, and G. Michelson. Glaucoma risk index: automated glaucoma detection from color fundus images. *Medical Image Analysis*, 14(3):471–481, 2010.

[6] C. Chang and C. Lin. Libsvm: a library for support vector machines. *Software available at http://www.csie.ntu.edu.tw/ cjlin/libsvm/*, 2001.

[7] J. Cheng, J. Liu, Y. Xu, F. Yin, D. W. Wong, N. M. Tan, D. Tao, C. Y. Cheng, T. Aung, and T. Y. Wong. Superpixel classification based optic disc and optic cup segmentation for glaucoma screening. *IEEE Trans Med Imaging*, June 2013.

[8] J. Cheng*, D. Tao, J. Liu, D. W. K. Wong, N.-M. Tan, T. Y. Wong, and S. M. Saw. Peripapillary atrophy detection by sparse biologically inspired feature manifold. *IEEE TRANSACTIONS ON MEDICAL IMAGING*, 2012.

[9] E. Corona. Digital stereo image analyzer for generating automated 3-d measures of optic disc deformation in glaucoma. *IEEE Transactions on Medical Imaging*, 21(10):1244–1253, 2002.

[10] K. S. Deepak, N. K. Medathati, and J. Sivaswamy. Detection and discrimination of disease-related abnormalities based on learning normal cases. *Pattern Recognition*, 2012.

[11] K. S. Deepak and J. Sivaswamy. Automatic assessment of macular edema from color retinal images. *IEEE Trans. Med. Imaging*, 2012.

[12] C. Fleming, W. E, T. Beil, and B. Smit. Primary care screening for ocular hypertension and primary open-angle glaucoma. *Agency for Healthcare Research and Quality, Available at: http://www.ahrq.gov/clinic/serfiles.htm*, 2005.

[13] C. Fleming, E. Whitlock, T. Beil, B. Smit, and R. Harris. Screening for primary open-angle glaucoma in the primary care setting: an update for the us preventive services task force. *Ann Fam Med*, 3::167–170, 2005.

[14] N. Harizman, C. Oliveira, A. Chiang, C. Tello, M. Marmor, R. Ritch, and J. M. Liebmann. The isnt rule and differentiation of normal from glaucomatous eyes. *Arch Ophthalmol*, pages 124(11):1579–83, Nov 2006.

[15] Y. Hatanaka, A. Noudo, C. Muramatsu, A. Sawada, T. Hara, T. Yamamoto, and H. Fujita. Automatic measurement of vertical cup-to-disc ratio on retinal fundus images. *ICMB*, pages 64–72, 2010.

[16] G. Joshi, J. Sivaswamy, and S. Krishnadas. Optic disk and cup segmentation from monocular colour retinal images for glaucoma assessment. *IEEE Transactions on Medical Imaging*, 30(6):1192–1205, 2011.

[17] G. Joshi, J. Sivaswamy, and S. Krishnadas. Depth discontinuity-based cup segmentation from multi-view colour retinal images. *IEEE Transactions on Biomedical Engineering*, 59(6):1523–1531, 2012.

[18] G. D. Joshi, J. Sivaswamy, R. Prashanth, and S. R. Krishnadas. Detection of peri-papillary atrophy and rnfl defect from retinal images. *ICIAR*, 2011.

[19] R. Kolar, J. Jan, R. Laemmer, and R. Jirik. Semiautomatic detection and evaluation of autofluorescent areas in retinal images. *Proc. EMBS*, pages 3327–3330, 2007.

[20] M. Lester, D. Garway-Heath, and H. Lemij. Optic nerve head and retinal nerve fibre analysis. *European Glaucoma Society*, 2005.

[21] V. Malinovsky. An overview of the heidelberg retina tomograph. *J. Am.Optom. Assoc*, 67(8):457467, 1996.

[22] A. McIntyre, M. Heywood, P. Artes, and S. Abidi. Toward glaucoma classification with moment methods. *Computer and Robot Vision*, pages 265–272, 2004.

[23] A. McIntyre, M. Heywood, S. A. P.H. Artes, and Y. Jin. Automated optic nerve analysis for diagnostic support in glaucoma. *Computer Based Medical Systems*, pages 97–102, 2005.

[24] N. V. K. Medathati and J. Sivaswamy. Local descriptor based on texture of projections. *ICVGIP*, 2010.

[25] C. Muramatsu, Y. Hatanaka, A. Sawada, T. Yamamoto, and H. Fujita. Computerized detection of peripapillary chorioretinal atrophy by texture analysis. *33rd Annual International Conference of the IEEE EMBS Boston, Massachusetts USA*, 2011.

[26] C. Muramatsu, T. Nakagawa, A. Sawada, Y. Hatanaka, T. Hara, T. Yamamoto, and H. Fujit. Determination of cup and disc ratio of optical nerve head for diagnosis of glaucoma on stereo retinal fundus image pairs. *SPIE*, 2009.

[27] M. Niemeijer, M. D. Abramoff, and B. van Ginneken. Image structure clustering for image quality verification of color retina images in diabetic retinopathy screening. *MIA*, 10:888–898, 2006.

[28] L. Nyl. Retinal image analysis for automated glaucoma risk evaluation. *SPIE: Medical Imaging*, 7497:74971C1, 2009.

[29] H. Ohwada, M. Daidoji, S. Shirato, and F. Mizoguchi. Learning first-order rules from image applied to glaucoma diagnosis. *International Conference on Artificial Intelligence: Topics in Artificial Intelligence*, pages 494–505, 1998.

[30] S. Philip, A. D. Fleming, K. G. A. S. Fonseca, P. Mcnamee, G. S. Scotland, G. J. Prescott, P. F. Sharp, and J. A. Olson. The efficacy of automated disease/no disease grading for diabetic retinopathy in a systematic screening programme. *Br J Ophthalmol.*, 91(11)::1512–1517, 2007.

[31] R. Saxena, D. Singh, and P. Vashist. Glaucoma: An emerging peril. *Indian Journal of Community Medicine*, 38(3):135–137, 2013.

[32] C. Shyu, C. Brodley, A. Kak, A. Kosaka, A. Aisen, and L. Broderick. Local versus global features for content-based image retrieval. in content-based access of image and video libraries. *Proceedings. IEEE Workshop*, pages 30–34, 1998.

[33] K. Stapor, A. Sacutewitonski, R. Chrastek, and G. Michelson. Segmentation of fundus eye images using methods of mathematical morphology for glaucoma diagnosis. *ICCS*, pages 41–48, 2004.

[34] D. Tao, F. Yin, D. Kee, Y. Xu, T. Yin, J. Cheng, and J. Liu. Superpixel classification based optic cup segmentation. *Medical Image Computing and Computer-assisted Intervention (MICCAI)*, 8151:421–428, 2013.

[35] D. Wong, J. Liu, J. Lim, H. Li, X. Jia, F. Yin, and T. Wong. Automated detection of kinks from blood vessels for optic cup segmentation in retinal images. *Proc. SPIE Medical Imaging*, page 72601J, 2009.

[36] D. Wong, J. Liu, J. Lim, H. Li, N. Tan, and T. Wong. Argali - an automatic cup-to-disc ratio measurement system for glaucoma detection and analysis framework. *Proc. SPIE Medical Imaging*, page 72603K, 2009.

[37] J. Xu. Optic disk feature extraction via modified deformable model technique for glaucoma analysis. *Pattern Recognition*, 40:2063–2076, 2007.